Pekka Alitalo and Sergei Tretyakov. 2007. Subwavelength resolution with three-dimensional isotropic transmission-line lenses. Metamaterials, volume 1, number 2, pages 81-88.

Available online at www.sciencedirect.com
ScienceDirect
Metamaterials 1 (2007) 81–88
Metamaterials
www.elsevier.com/locate/metmat

Subwavelength resolution with three-dimensional isotropic transmission-line lenses

Pekka Alitalo*, Sergei Tretyakov

Radio Laboratory/SMARAD Center of Excellence, TKK Helsinki University of Technology, P.O. Box 3000, FI-02015 TKK, Finland

Received 4 May 2007; received in revised form 22 August 2007; accepted 2 September 2007
Available online 6 September 2007

Abstract

Dispersion, impedance matching and resolution characteristics of an isotropic three-dimensional flat lens ("superlens") are studied. The lens is based on cubic meshes of interconnected transmission lines and lumped loads. We study a practical realization of the lens, based on the microstrip technology. The dispersion equations that have been previously derived, are verified with full-wave simulations. The isotropy of the structure is verified with analytical as well as simulation results. The resolution characteristics of a practically realizable, lossy lens are studied analytically.

PACS: 42.30. −d; 42.30.Wb

Keywords: Transmission-line network; Dispersion; Isotropy; Subwavelength resolution

1. Introduction

Materials with simultaneously negative material parameters (double-negative or backward-wave materials, where permittivity ε and permeability μ are both effectively negative) [1] have received a lot of interests in the recent literature. One of the most exciting applications of these materials is a device capable of subwavelength resolution (resolution that exceeds the diffraction limit) [2]. The first demonstrations of realized artificial backward-wave materials were done in the microwave region using periodic structures consisting of metal wires (negative ε) and split-ring resonators (negative μ) [3].

Also the use of loaded transmission-line networks has been proposed for the realization of wideband and low-loss backward-wave materials in the microwave region [4,5]. These networks are inherently one- or two-dimensional structures [6,7]. Recently, also three-dimensional, isotropic transmission-line-based backward-wave materials have been proposed [8–10] and realized [11]. For a thorough explanation of the mechanisms of evanescent wave enhancement and focusing of propagating waves in this type of structures see e.g. [12,13].

It has been shown that subwavelength imaging of the near-field is possible even without backward-wave materials (note that in these cases the focusing of the propagating modes is not possible). This phenomenon can be achieved with a slab of material having negative permittivity or permeability [14], or without any volumetric material slab by using planar sheets supporting

* Corresponding author. Fax: +358 9 451 2152.
E-mail address: pekka.alitalo@tkk.fi (P. Alitalo).

1873-1988/$ – see front matter © 2007 Elsevier B.V. All rights reserved.
doi:10.1016/j.metmat.2007.09.001

surface plasmons [15–17]. Also devices which operate in the "canalization" regime have been used successfully to obtain subwavelength resolution [18,19]. Here "canalization" refers to the transfer of evanescent modes into propagating modes. Some of the previous methods have also been suggested for use in the optical region [14,20,21].

The current paper is devoted to a detailed study of a three-dimensional, isotropic superlens based on loaded transmission-line networks. This approach to superlens design was originally proposed in Ref. [10] and experimentally confirmed in Ref. [11]. In Ref. [10], the basic design equations for unloaded and loaded transmission-line networks were given and applied in the design of a superlens composed of these networks. In Ref. [11] an experimental realization of the same design was presented. In earlier papers, the isotropy of the structure was assumed since the period of the structure is much smaller than the wavelength of the waves travelling in the networks. Here it must be noted that by the term "isotropy" we refer to the isotropic propagation of scalar waves of voltages and currents. The notion of polarization of waves is not applicable here because the source is embedded in a transmission-line network where waves are also scalar. Furthermore, the resolution characteristics, such as resolution enhancement and achievable bandwidths of realizable designs, were not studied in Refs. [10,11].

In this paper, we further confirm the isotropy of the structure by studying the dependence of the dispersion on the direction of propagation and verify the analytical design equations presented in Ref. [10] with full-wave simulations. We also confirm that the impedance matching, which is essential for operation of the device, is preserved for all directions of propagation. The resolution enhancement capability of a practically realizable, three-dimensional lossy lens is analytically studied using a method presented and applied for the case of a two-dimensional lens in Ref. [22]. Although the lens inherently achieves ideal operation at a single frequency only (the dispersion curves of forward-wave and backward-wave networks intersect at a single frequency point), we show that the enhancement of the evanescent modes, which enables subwavelength resolution, is possible in a small but finite frequency band near the optimal operation frequency. An example case is studied analytically with taking into account realistic losses and the image formed by the proposed superlens is compared to a diffraction-limited image, which comprises only propagating modes.

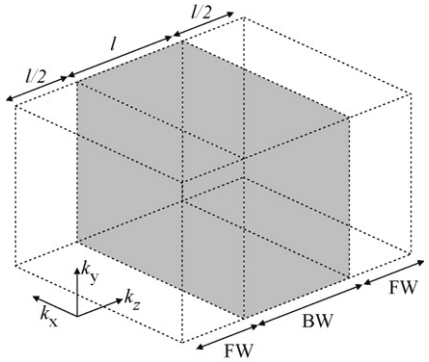

Fig. 1. Structure of the superlens. The distance between the source and image planes is $2l$.

2. The structure of the lens and dispersion in loaded and unloaded transmission-line networks

We study the superlens structure presented in Refs. [10,11]. The superlens is a combination of two types of transmission-line networks: a region with effectively negative ε and μ is sandwiched between two regions possessing effectively positive ε and μ (forward-wave regions) (see Fig. 1). As was previously shown in Ref. [10], the transmission-line networks are easy to realize using the microstrip technology and we continue to use this approach in this paper (the design equations can be applied to other types of transmission lines as well, see [10]). The forward-wave and backward-wave networks have unit cells as shown in Fig. 2. The unit cell of the backward-wave network is otherwise similar to the forward-wave unit cell, but it is loaded with lumped capacitors of value $2C$ (in series with the microstrip lines) in all of the six branches of the unit cell and an inductor of value L is connected from the center node of the microstrip line to the ground.

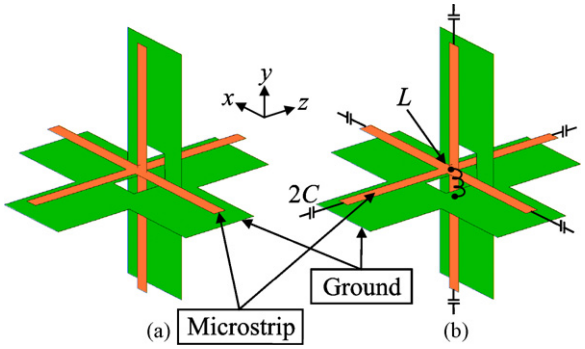

Fig. 2. Unit cells of three-dimensional forward-wave (a) and backward-wave (b) transmission-line networks based on the microstrip technology (the substrate is not shown for clarity).

The dispersion equations for the forward-wave and backward-wave networks have been derived in Ref. [10] and they read (in the lossless case):

$$\cos(q_x)+\cos(q_y)+\cos(q_z)=\frac{1}{2j\omega L S_{\mathrm{BW}}}-3\frac{K_{\mathrm{BW}}}{S_{\mathrm{BW}}} \quad (1)$$

and

$$\cos(q_x)+\cos(q_y)+\cos(q_z)=-3\frac{K_{\mathrm{FW}}}{S_{\mathrm{FW}}}, \quad (2)$$

where

$$S_{\mathrm{BW}}=\frac{j\omega C}{(D_{\mathrm{TL}}+j\omega C B_{\mathrm{TL}})(A_{\mathrm{TL}}+j\omega C B_{\mathrm{TL}})+\omega^2 C^2 B_{\mathrm{TL}}^2}, \quad (3)$$

$$K_{\mathrm{BW}}=\frac{-(B_{\mathrm{TL}}C_{\mathrm{TL}}-D_{\mathrm{TL}}A_{\mathrm{TL}})(A_{\mathrm{TL}}+j\omega C B_{\mathrm{TL}})}{[(D_{\mathrm{TL}}+j\omega C B_{\mathrm{TL}})(A_{\mathrm{TL}}+j\omega C B_{\mathrm{TL}})+\omega^2 C^2 B_{\mathrm{TL}}^2]B_{\mathrm{TL}}}-\frac{A_{\mathrm{TL}}}{B_{\mathrm{TL}}}, \quad (4)$$

$$S_{\mathrm{FW}}=\frac{1}{B_{\mathrm{TL}}(A_{\mathrm{TL}}+D_{\mathrm{TL}})} \quad (5)$$

$$K_{\mathrm{FW}}=-\frac{B_{\mathrm{TL}}C_{\mathrm{TL}}-D_{\mathrm{TL}}A_{\mathrm{TL}}}{A_{\mathrm{TL}}+D_{\mathrm{TL}}}\frac{1}{B_{\mathrm{TL}}}-\frac{A_{\mathrm{TL}}}{B_{\mathrm{TL}}}, \quad (6)$$

$$\begin{bmatrix} A_{\mathrm{TL}} & B_{\mathrm{TL}} \\ C_{\mathrm{TL}} & D_{\mathrm{TL}} \end{bmatrix} = \begin{bmatrix} \cos(k_{\mathrm{TL}}d/2) & jZ_{0,\mathrm{TL}}\sin(k_{\mathrm{TL}}d/2) \\ jZ_{0,\mathrm{TL}}^{-1}\sin(k_{\mathrm{TL}}d/2) & \cos(k_{\mathrm{TL}}d/2) \end{bmatrix}. \quad (7)$$

In (1)–(6) the indices FW and BW correspond to the dispersion equations of forward-wave and backward-wave networks, respectively, and $q_i = k_i d$ (wave number normalized by the period d), where k_i is the wave number in the network along axis i. In (7) k_{TL} and $Z_{0,\mathrm{TL}}$ are the wave number and impedance of the waves in the transmission lines, respectively. Note that $Z_{0,\mathrm{TL}}$ is usually different for the forward-wave and backward-wave networks in order to obtain impedance matching of the networks [10].

The parameters of the structure that is studied here are the same as in Ref. [11](see Table 1, ε_{r} is the permittivity of the substrate of the microstrip lines). Dispersion curves of the forward-wave and backward-wave networks can be studied analytically using (1)–(7). The unit cells of the both networks have also been simulated with Ansoft HFSS full-wave simulator to obtain the dispersion curves for both networks. See Fig. 3 for the dispersion curves when a planewave is considered ($k_x = k_y = 0$). The simulation results agree very well for plane wave propagation in all axial directions (practically identical plots). From Fig. 3 we can conclude that the optimal operation frequency of the superlens is $f = 0.8513$ GHz (the frequency at which the dispersion curves intersect) and at that point the wave number has value $k_z \approx 47.65\,\mathrm{m}^{-1}$.

From (1) and (2) we clearly see that if we consider diagonal propagation (k_x, k_y and k_z may all be nonzero depending on the direction of propagation), this introduces some anisotropy to the dispersion. To study this effect, we have analyzed propagation in the structure in other than the axial directions. It has been seen that for the backward-wave network the isotropy is achieved in a large bandwidth below and above the second stopband (for this example, the isotropic region is approximately from 0.5 to 2 GHz), and for the forward-wave network at low frequencies (for this example, below 2 GHz). The operation frequency of the designed lens is well within this isotropic region for both networks. The optimal operation frequency obtained here differs slightly from the one previously presented for a similar structure [11]. The reason for this is that here we have assumed the effec-

Table 1
Parameters of the superlens structure

d (mm)	13
$Z_{0,\mathrm{TL,FW}}$ (Ω)	66
$Z_{0,\mathrm{TL,BW}}$ (Ω)	89
C (pF)	3.3
L (nH)	6.8
ε_{r}	2.33

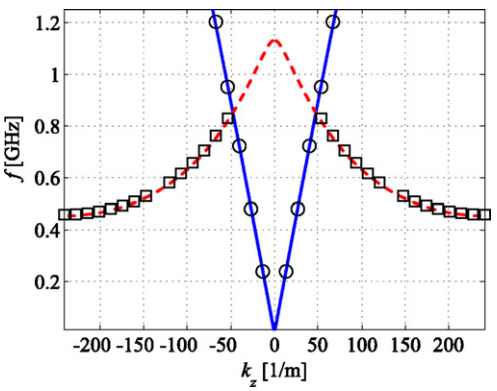

Fig. 3. Dispersion curves for the forward-wave (solid line: analytical; circles: HFSS) and backward-wave (dashed line: analytical; squares: HFSS) networks. Propagation along the z-axis is considered ($k_x = k_y = 0$).

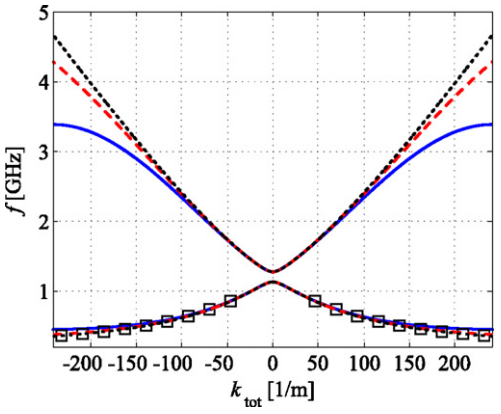

Fig. 4. Dispersion curves for the backward-wave network. Solid line: $k_x = k_y = 0$; dashed line: $k_y = 0$, $k_x = k_z$; dotted line: $k_x = k_y = k_z$; squares: $k_x = k_y = k_z$ (HFSS).

tive permittivity of the transmission lines to be equal to ε_r (to simplify comparison between the analytical and simulation results).

See Figs. 4 and 5 for the results considering different propagation directions. The analytical results (solid, dashed and dotted lines) are compared to the results obtained from HFSS simulation models with the geometry as shown in Fig. 2. Note that for the diagonal propagation, the dispersion curves extend to larger values of $k_{\text{tot}} = \sqrt{k_x^2 + k_y^2 + k_z^2}$ than it is shown in Figs. 4 and 5 (these regions are not of interest for superlens operation). The HFSS simulation results agree very well for all of the presented curves. For clarity only the diagonal propagation corresponding to the case with $k_x = k_y = k_z$ is presented (squares and circles). The results shown in Figs. 4 and 5 justify our assumption of

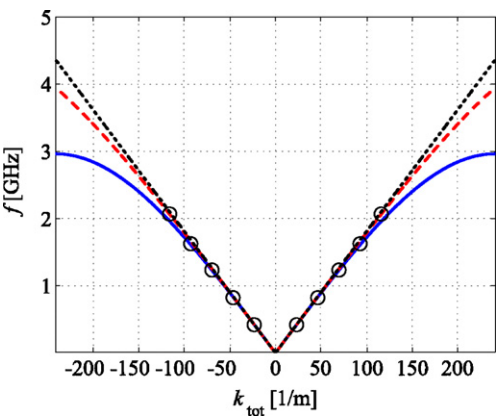

Fig. 5. Dispersion curves for the forward-wave network. Solid line: $k_x = k_y = 0$; dashed line: $k_y = 0$, $k_x = k_z$; dotted line: $k_x = k_y = k_z$; circles: $k_x = k_y = k_z$ (HFSS).

isotropy proposed in Ref. [11] for the microstrip network. Although the *xy*-, *xz*- and *yz*-planes are inherently different due to the use of the microstrip technology, the focusing of a source can be obtained in any plane simply because the scalar waves of voltages and currents do not see any difference between the various directions of propagation.

3. Impedance matching

As was shown in Refs. [10,11], the impedance matching is crucial for the operation of the superlens. Here we use the equations derived for the characteristic impedances of the forward-wave and backward-wave networks [10] to see if the matching is preserved for all propagation directions. In the following we study the matching analytically and tune the impedances of the transmission lines slightly to obtain optimal resolution performance (in Ref. [11] and in the previous section the impedance values were not ideal due to the fact that the values were taken from an experimental prototype). It was found that by changing the impedance of the forward-wave transmission lines to $Z_{0,\text{TL,FW}} = 69.46\,\Omega$, the wave numbers and the characteristic impedances of the networks can be matched at the frequency $f = 0.8513$ GHz. In the rest of this paper, we use this impedance value and the other design characteristics stay the same as shown in Table 1.

See Fig. 6 for the characteristic impedances of the both networks for different propagation directions. Note that because we are interested in the matching between the two networks, the characteristic impedance is defined as the ratio of the voltage and the *z*-component of the current (as was done in Refs. [10,11]). We see that although the values of the impedances change as the direction of propagation changes (naturally, because the impedance

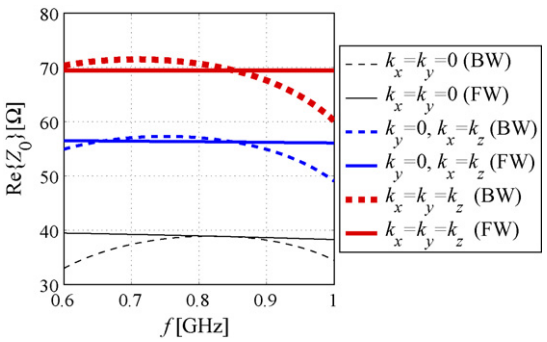

Fig. 6. The characteristic impedances of forward-wave and backward-wave networks for different propagation directions.

depends on k_z), the matching is preserved for different propagation directions at the operation frequency ($f = 0.8513$ GHz).

4. Resolution characteristics

4.1. Resolution enhancement

To evaluate the performance of the designed lens, we adopt the same method of calculating the resolution enhancement as in Ref. [22], where the resolution enhancement was defined for a two-dimensional (planar) lens as

$$R_e = \frac{k_{t,\max}}{k_{\text{eff}}}, \tag{8}$$

where $k_{t,\max}$ is the maximum transverse wave number that is transmitted from the source plane to the image plane and k_{eff} is the maximum wave number corresponding to propagating modes ($k_{\text{eff}} \approx 47.65\ \text{m}^{-1}$ at $f = 0.8513$ GHz for the lens that we study here). Because we consider a three-dimensional lens, the transverse wave number is now defined as $k_t = \sqrt{k_x^2 + k_y^2}$ (see Fig. 1).

In Ref. [22], $k_{t,\max}$ was derived analytically from the dimensions of the used superlens (taking into account the effect of losses) as well as calculated from the optical transfer function that was derived analytically and also measured. It was concluded that a good approximation for $k_{t,\max}$ is the value of k_t, at which the absolute value of the optical transfer function drops to 0.5 [22]. In the following, we calculate the transmission coefficient of the lens studied in this paper using the previously derived equations [10]. From the absolute value of the transmission coefficient (which corresponds to the optical transfer function used in Ref. [22]) we obtain R_e by finding $k_{t,\max}$ from the plotted curves as described above. The theoretical maximum of R_e for the example lens studied in this paper is (at the frequency $f = 0.8513$ GHz)

$$R_{e,\max} = \frac{\pi}{dk_{\text{eff}}} \approx 5. \tag{9}$$

First, let us see how the thickness of the superlens affects the resolution enhancement. We have calculated the resolution enhancement for the superlens described in the previous sections, taking into account realistic losses caused by the substrate and by the lumped elements (loss tangent of the substrate is $\tan\delta = 0.0012$ and the quality factors of the capacitors and inductors are $Q_C = 500$ and $Q_L = 50$, respectively) [11]. In the calculations, the losses can be taken into account by using complex values for C and L and by replacing (7) by

$$\begin{bmatrix} A_{\text{TL}} & B_{\text{TL}} \\ C_{\text{TL}} & D_{\text{TL}} \end{bmatrix} = \begin{bmatrix} \cosh(\gamma d/2) & jZ_{0,\text{TL}} \sinh(\gamma d/2) \\ jZ_{0,\text{TL}}^{-1} \sinh(\gamma d/2) & \cosh(\gamma d/2) \end{bmatrix}, \tag{10}$$

where

$$\gamma = \frac{\pi\varepsilon_r(\varepsilon_r - 1)\tan\delta}{\sqrt{\varepsilon_r}(\varepsilon_r - 1)\lambda_0} + jk_{\text{TL}} \tag{11}$$

and λ_0 is the wavelength in free space.

See Fig. 7 for the resolution enhancement as a function of the distance between the source and image planes (this distance is equal to two times the thickness of the lens l). Note that when we find $k_{t,\max}$ for different thicknesses, the "worst case" is always used. Because of the fact that the impedance values are different for different directions of propagation (see Fig. 6), $k_{t,\max}$ is slightly different for various propagation directions. It was found that for the lens studied in this paper $|k_{t,\max}|$ is smallest for the case when $k_x = k_y$, i.e., $k_t = \sqrt{k_x^2 + k_y^2} = \sqrt{2k_x^2}$. In the calculation of Fig. 7 and in Section 4.2 this "worst case" is used to calculate R_e.

In Fig. 7, an approximation for the resolution enhancement is also plotted. This approximation can be found from Ref. [22] and it is calculated with

$$R_{e,\text{approx}} = \frac{\ln(Q_C)}{lk_{\text{eff}}}. \tag{12}$$

R_e calculated from the transmission coefficient data (circles in Fig. 7) and R_e calculated from the approximate

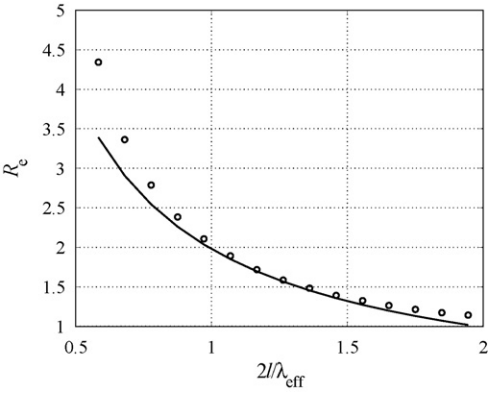

Fig. 7. Resolution enhancement of the studied lens, as a function of the distance between source and image (in wavelengths at the optimal operation frequency, $f = 0.8513$ GHz). Circles: R_e calculated from the transmission coefficient data (losses of the substrate and the lumped components are taken into account). Solid line: approximation for R_e, calculated using the equation from Ref. [22].

equation (solid line in Fig. 7) are in fairly good correspondence with each other, especially when the distance between the source and image is around one wavelength. There is no motivation to calculate the resolution enhancement for values $2l < 0.5\lambda_{\text{eff}} = \pi/k_{\text{eff}}$, because then the image would be very close to the source and some of the evanescent modes would contribute to the image formation even without any superlens. It can also be concluded that when the distance between the source and image becomes larger than one wavelength, the resolution enhancement of the lens is considerably degraded and reaches the value 1 (i.e., the superlens offers no enhancement of resolution at all) approximately when the distance between the source and image is $2\lambda_{\text{eff}}$.

4.2. Bandwidth

Ideal operation of the superlens described in this paper can be achieved only at a single frequency, as can be seen from Fig. 3. Nevertheless, it is clear that although a small change in the frequency distorts the image seen in the image plane, focusing of the propagating modes and enhancement of the evanescent modes are still expected to happen in some small but finite frequency band. Here we rely on the assumption that the resolution enhancement can still be defined with (8), i.e., the distortion of the image is not very dramatic and $k_{t,\max}$ can still be defined as described above. In the following, the operation band is defined as the frequency band where $R_{\text{e}} > 2$.

First, let us study a lens with the thickness of the backward-wave network being $l = 4d$ and the distance between the source and image planes being $2l = 8d$. In wavelengths this is $0.79\lambda_{\text{eff}}$ at the center frequency ($f = 0.8513$ GHz), because $\lambda_{\text{eff}} = 2\pi/k_{\text{eff}} \approx 0.132$ m. See Fig. 8 for a plot of the transmission coefficient (the absolute value), calculated for the center frequency as well as for lower and higher frequencies that still satisfy the previously defined condition $R_{\text{e}} > 2$. From Fig. 8 we see that the operation band is approximately 2%. When the frequency deviates from the optimal value, there occur peaks of transmission right before the transmission starts to go down very quickly. We believe that this peaking is caused by the inevitable mismatches between the two types of transmission-line networks (the optimal matching of the wave numbers and network impedances can be obtained only at a single frequency).

By making the lens thinner, the bandwidth can be improved. For a lens with thickness l equal to three times the period d (the distance between the source and the image equals to $6d \approx 0.59\lambda_{\text{eff}}$), the bandwidth where $R_e > 2$ is found to be approximately 6%.

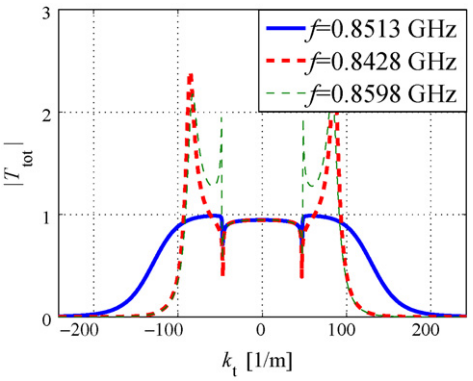

Fig. 8. Transmission from the source plane to the image plane as a function of the transverse wave number. The band where $R_{\text{e}} > 2$ is approximately 2%. The distance between the source and image planes equals $0.79\lambda_{\text{eff}}$ at the center frequency.

To demonstrate the resolution characteristics of the designed lens, we calculate the image formed by the lens for a source with subwavelength features. We use a line source that is placed diagonally with respect to the x- and y-axis (i.e., the source lies along the line $y = -x$). The source includes harmonics in the range $-100 < k_t < 100$, with the amplitude of all the harmonics being equal. We use the same lens thickness as in Fig. 8, i.e., the lens thickness is $4d$ and the distance between the source and the image is $8d = 0.79\lambda_{\text{eff}}$. We calculate the source and image plane voltage distributions at the three frequencies shown in Fig. 8.

Fig. 9 shows the voltage distributions in the source and image planes, all normalized to the maximum voltage in the source plane. Also, the image formed by a diffraction-limited lens is plotted (for this image, only the propagating modes are focused in the image and all the evanescent modes are strongly attenuated). The voltages are calculated at the nodal positions of the transmission-line network. From Fig. 9 we can conclude that all the image plane distributions with the superlens Fig. 9(b)–(d) are very close to the source plane distribution (Fig. 9(a)), although in Fig. 9(c) and (d) the sidelobe level of the image is somewhat higher than that in the source plane distribution. The image plane distribution with a diffraction-limited lens on the other hand is strongly attenuated in the amplitude, and the beamwidth is clearly wider than in the source plane distribution.

To further illustrate the resolution enhancement effect, we have plotted the source and image plane field intensities for different frequencies along a single line (see Fig. 10). Because we use the diagonally positioned line source (see Fig. 9(a)) we have plotted the field intensities along a line $x = y$. The field is calculated at the nodal positions of the transmission-line network. There-

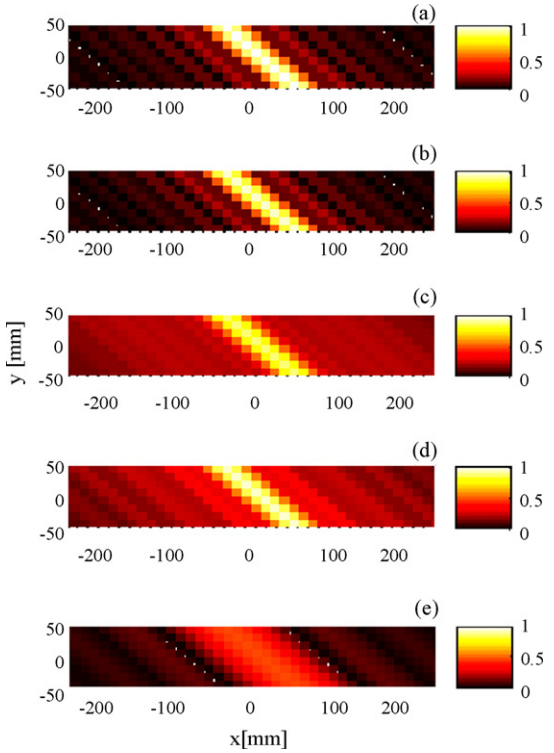

Fig. 9. Voltage distributions (normalized to the maximum in the source plane). (a) Source plane; (b) image plane, $f = 0.8513$ GHz; (c) image plane, $f = 0.8428$ GHz; (d) image plane, $f = 0.8598$ GHz; and (e) image plane with a diffraction-limited lens.

fore, the distance between the adjacent points in which the field is calculated is $\sqrt{2d^2} \approx 18.4$ mm. All the plots have been normalized to their maximum intensities. If we normalize all the plots to the peak intensity in the source plane, we can accurately study the effect of losses on the image amplitude: for frequency $f = 0.8513$ GHz the image peak intensity is approximately 89% of that of the source, and for $f = 0.8428$ and 0.8598 GHz they are 74% and 89%, respectively. For the diffraction-limited case the image peak intensity is only 23% of the peak intensity in the source plane.

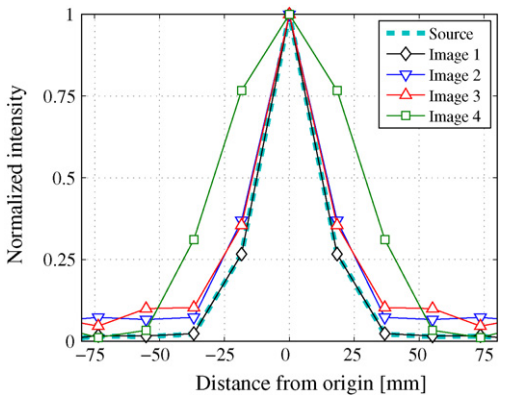

Fig. 10. Normalized intensities in the source and image planes. Image 1: $f = 0.8513$ GHz; image 2: $f = 0.8428$ GHz; image 3: $f = 0.8598$ GHz; and image 4: diffraction-limited. The distance between the source and image planes equals $0.79\lambda_{\text{eff}}$ at the center frequency.

From Fig. 10 we can conclude that the field pattern of the source plane is well preserved in the image plane for the shown three frequencies when the superlens is used. The diffraction-limited image, on the other hand, has a half-power beamwidth of approximately two times those of the images formed by the superlens.

It must also be noted, that at least in this case, the distortion of the transmission coefficient (the peaking of the transmission coefficient was discussed earlier) does not destroy the imaging effect. The effect of the peaking can nevertheless be seen from the plots in Fig. 10; the images at the lower and higher frequencies clearly have some of the higher harmonics enhanced too much (the sidelobe level is increased as compared with the image at the optimal frequency).

5. Conclusions

We have extended the study of a previously proposed superlens based on loaded and unloaded three-dimensional isotropic transmission-line networks. We have verified the previously derived dispersion equations by full-wave simulations and have shown that the designed structure is isotropic in all propagation directions (not just along the three axial ones). We have also confirmed that impedance matching of the two types of networks is possible for an arbitrary direction of propagation. We have analytically studied the effect of losses and the thickness of the lens on the resolution and bandwidth characteristics of a realizable device. When high-quality and low-loss components and materials are used, the designed lens can achieve substantial resolution enhancement in a relative bandwidth of a few percent, with the distance between the source and the image being of the order of one wavelength.

Acknowledgements

This work has been partially funded by the Academy of Finland and TEKES through the Center-of-Excellence program. The authors wish to thank Tero Kiuru and Olli Luukkonen for helpful discussions regarding the simulation software. P.A. wishes to thank the Graduate School in Electronics, Telecommunications and Automation (GETA) and the Nokia Foundation for financial support.

References

[1] V.G. Veselago, The electrodynamics of substances with simultaneously negative values of ε and μ, Sov. Phys. Usp. 10 (1968) 509–514.

[2] J.B. Pendry, Negative refraction makes a perfect lens, Phys. Rev. Lett. 85 (2000) 3966–3969.

[3] R.A. Shelby, D.R. Smith, S. Schultz, Experimental verification of a negative index of refraction, Science 292 (2001) 77–79.

[4] C. Caloz, H. Okabe, T. Iwai, T. Itoh, Transmission line approach of left-handed (LH) materials, in: Proceedings of the USNC/URSI National Radio Science Meeting, San Antonio, TX 1, 2002, p. 39.

[5] G.V. Eleftheriades, A.K. Iyer, P.C. Kremer, Planar negative refractive index media using periodically *L–C* loaded transmission lines, IEEE Trans. Microw. Theor. Tech. 50 (2002) 2702–2712.

[6] C. Caloz, T. Itoh, Transmission line approach of left-handed (LH) materials and microstrip implementation of an artificial LH transmission line, IEEE Trans. Antennas Propag. 52 (2004) 1159–1166.

[7] A. Grbic, G.V. Eleftheriades, Overcoming the diffraction limit with a planar left-handed transmission-line lens, Phys. Rev. Lett. 92 (2004) 117403.

[8] A. Grbic, G.V. Eleftheriades, An isotropic three-dimensional negative-refractive-index transmission-line metamaterial, J. Appl. Phys. 98 (2005) 043106.

[9] W.J.R. Hoefer, P.P.M. So, D. Thompson, M.M. Tentzeris, Topology and design of wide-band 3D metamaterials made of periodically loaded transmission line arrays, in: Proceedings of the 2005 IEEE MTT-S International Microwave Symposium Digest, 2005, pp. 313–316.

[10] P. Alitalo, S. Maslovski, S. Tretyakov, Three-dimensional isotropic perfect lens based on *LC*-loaded transmission lines, J. Appl. Phys. 99 (2006) 064912.

[11] P. Alitalo, S. Maslovski, S. Tretyakov, Experimental verification of the key properties of a three-dimensional isotropic transmission-line superlens, J. Appl. Phys. 99 (2006) 124910.

[12] G.V. Elefheriades, K.G. Balmain, Negative-Refraction Metamaterials: Fundamental Principles and Applications, John Wiley & Sons, Hoboken, NJ, 2005.

[13] C. Caloz, T. Itoh, Electromagnetic Metamaterials: Transmission Line Theory and Microwave Applications, John Wiley & Sons, Hoboken, NJ, 2006.

[14] N. Fang, H. Lee, C. Sun, X. Zhang, Sub-diffraction-limited optical imaging with a silver superlens, Science 308 (2005) 534–537.

[15] S. Maslovski, S.A. Tretyakov, P. Alitalo, Near-field enhancement and imaging in double planar polariton-resonant structures, J. Appl. Phys. 96 (2004) 1293–1300.

[16] M.J. Freire, R. Marqués, Planar magnetoinductive lens for three-dimensional subwavelength imaging, Appl. Phys. Lett. 86 (2005) 182505.

[17] P. Alitalo, S. Maslovski, S. Tretyakov, Near-field enhancement and imaging in double planar polariton-resonant structures: enlarging superlens, Phys. Lett. A 357 (2006) 397–400.

[18] P.A. Belov, C.R. Simovski, P. Ikonen, Canalization of subwavelength images by electromagnetic crystals, Phys. Rev. B 71 (2005) 193105.

[19] P. Ikonen, P. Belov, C. Simovski, S. Maslovski, Experimental demonstration of subwavelength field channeling at microwave frequencies using a capacitively loaded wire medium, Phys. Rev. B 73 (2006) 073102.

[20] A. Alù, N. Engheta, Optical nanotransmission lines: synthesis of planar left-handed metamaterials in the infrared and visible regimes, J. Opt. Soc. Am. B 23 (2006) 571–583.

[21] P. Alitalo, C. Simovski, A. Viitanen, S. Tretyakov, Near-field enhancement and subwavelength imaging in the optical region using a pair of two-dimensional arrays of metal nanospheres, Phys. Rev. B 74 (2006) 235425.

[22] A. Grbic, G.V. Eleftheriades, Practical limitations of subwavelength resolution using negative-refractive-index transmission-line lenses, IEEE Trans. Antennas Propag. 53 (2005) 3201–3209.